

DCM and CCM Operation of Buck-Boost Full-Bridge DC-DC Converter

Niraja Swaminathan¹, *Member, IEEE*, Lakshminarasamma N², *Member, IEEE* and Yue Cao¹, *Member, IEEE*

¹School of Electrical Engineering and Computer Science, Oregon State University, USA

²Department of Electrical Engineering, Indian Institute of Technology Madras, India

Abstract—Buck-Boost based full-bridge DC-DC converters possess potentials for high gain, high power applications, particularly in solar PV, battery, and fuel-cell fed systems, as the converters feature non-pulsating input and output currents. However, these converters lack attention due to the presence of DC-current in the transformer winding. In this paper, a novel Buck-Boost full-bridge (BBFB) converter with a hybrid control scheme (HCS) mitigating the transformer DC-current is presented. The BBFB converter exhibits inherent soft-switching such that zero voltage switching (ZVS) conditions apply for individual switches. This paper analyzes the BBFB converter extensively, including the discontinuous conduction mode (DCM) operation and the DCM boundary condition. A dynamic behavior of the BBFB converter under a load step change verifies that the HCS scheme does not affect the converter performance. Besides, this work presents a model for the high frequency oscillations that occur in the practical transformer current waveform due to parasitic capacitances. All the analyses and the developed models are verified in simulations and hardware experiments. The developed models are useful for designing the BBFB converter with improved efficiency by ensuring the ZVS operation. Further, the developed models and results provide an insight for the DC voltage gain variations during DCM and continuous conduction mode (CCM). This helps the designer to choose the BBFB converter's operating mode based on the requirement.

Keywords—DC-DC converters, Full-bridge, zero voltage switching, discontinuous conduction mode, DC-current, and dynamic response

I. INTRODUCTION

High gain DC-DC converters are emerging in applications such as aviation distribution systems, electric vehicles, satellite power systems, and solar PV fed loads as they are essential to connect solar PV, battery, and fuel-cell to the DC bus [1]. These applications prefer isolated DC-DC converters to ensure equipment/human safety and avoid fault propagation [2]. Besides, the DC-DC converters must draw a continuous/non-pulsating current from the sources for reliable and efficient operation. Therefore, a careful selection of the high gain DC-DC converter is required [3].

Stable operation, reduced voltage and current stresses, high reliability, and soft-switching nature of full-bridge (FB) converters make the FB family promising for high gain, high power applications [4, 5]. Several FB topologies are presented in the literature and are broadly categorized into three types: Boost, Buck, and Buck-Boost [1, 2, 6–8]. The DC voltage gain is greater than unity in Boost-type FB converters under a unity transformer turns ratio, lesser than unity in buck-type converters, while greater or lesser than unity based on the operating duty ratio in Buck-Boost-type converters.

However, in most FB converters, the gain can be adjusted by an appropriate transformer turns ratio.

Most of the topologies presented under Boost- and Buck-types have either input or output pulsating currents, increasing the burden of filter capacitors, and also impacting the lifetime of sensitive sources or loads. In contrast, some Buck-Boost converters [1, 9–11] have non-pulsating input/output currents, making a potential choice for the above applications. A Buck-Boost topology in [9] has two input inductors connected to either pole point of the H-bridge, featuring low EMI, inherent soft-switching, and improved symmetry between the switches. However, this topology is limited from high power applications due to the presence of a DC-current in the transformer primary winding. Another variant of the Buck-Boost converter mitigates the transformer DC-current by using a series-connected capacitor [10]. However, this topology is not suitable for high input current applications due to a high capacitor RMS current requirement and an increased transformer primary peak current.

A Buck-Boost full-bridge (BBFB) converter with a simple control, namely hybrid control scheme (HCS), is presented in [1] to mitigate the transformer DC-current. BBFB is inspired from the basic boost converter and phase-shift full-bridge (PSFB) converter, featuring high power capability, high transformer utilization factor, inherent soft-switching, reduced component count, and twice the DC voltage gain as PSFB. The HCS control features independent control of the transformer DC-current while not affecting the output voltage control, thereby retaining the behavior of the converter. However, the analytical model of the converter other than the continuous conduction mode (CCM) operation is yet to be explored. Besides, the dynamic response of the HCS control is not available, and the zero voltage switching ZVS conditions for the input devices are unknown.

This paper presents a detailed analysis and model of the BBFB converter, beyond CCM. This study aids the designer in understanding the behavior of the converter in discontinuous conduction mode (DCM) using the developed DC voltage gain model. Also, the boundary condition for the CCM and DCM operation is derived. In this work, the ZVS conditions for all the input devices are proposed, which is useful for improving efficiency, particularly at low power. This work also derives a model for the resonant frequency of the parasitic capacitance and leakage inductance of the transformer, related to the ringing in the primary current. In the simulations, the dynamic performance of HCS under a load step change is evaluated. Hardware experimental results verifying the proposed models are presented.

The rest of the paper is organized as follows. Section II presents a steady-state model and analysis of the BBFB converter in DCM. The validation of the same and dynamic performance of the HCS control are presented in Section III. Section IV concludes the work.

II. STEADY-STATE ANALYSIS AND MODEL OF BBFB CONVERTER

The circuit diagram of BBFB with a high-level HCS control is shown in Fig. 1. The HCS control consists of two independent loops - DC-current mitigation and output regulation, where under steady-state, one loop does not affect the other's behavior. The DC-current mitigation loop uses the leading leg's (S_2 and S_3) asymmetrical duty D^* to nullify the DC-current in the transformer primary winding, while the output regulation loop uses the phase-shift ϕ between these legs to control the output voltage, as shown in Fig. 2. Therefore, the HCS control operates the lagging leg devices S_1 and S_4 at a fixed 50% duty ratio while switching the leading leg devices S_2 and S_3 asymmetrically with a phase-shift of ϕ with respect to the lagging leg, as shown in Fig. 3. Even though the operation of HCS is presented in [1], the behavior of the two loops under dynamic conditions is yet to be explored.

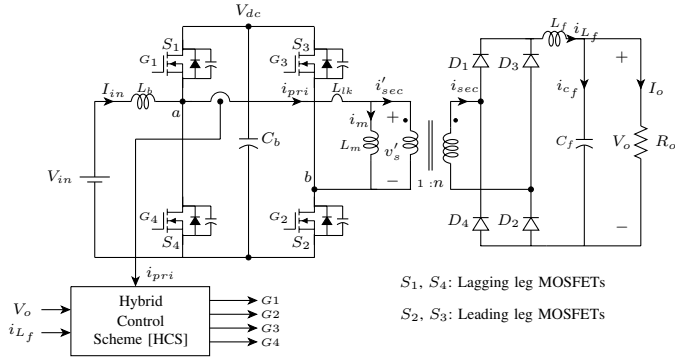


Fig. 1: BBFB converter with HCS

For a wide operating load range, BBFB can operate in DCM at a light load condition. Therefore, knowledge of the model and behavior of BBFB in DCM is necessary, which is presented next.

A. DCM operation of BBFB

The operation and analysis of BBFB in CCM are explained in [1]. The BBFB operation in DCM is similar to CCM during the power transfer and free-wheeling modes. However, DCM operation does not have transition modes, instead, additional zero-current intervals T_{i3} and T_{i6} exist. Fig. 4 presents the steady-state characteristic waveforms of the BBFB converter during DCM operation.

In the free-wheeling intervals T_{i2} and T_{i5} in DCM operation, the energy stored in the inductor L_f is less due to less output current I_o . This results in the inductor current i_{L_f} fall to zero. Subsequently, the BBFB converter enters the zero-current intervals T_{i3} and T_{i6} before the next power transfer intervals

T_{i4} and T_{i1} , respectively. During the zero-current intervals, the transformer primary current also remains zero. However, the input inductor current I_{in} can still be continuous. As the behavior of BBFB changes, the DC voltage gain in DCM is different from CCM.

B. DC voltage gain of BBFB in DCM

This subsection presents the DC voltage gain of BBFB in DCM operation. The model is derived based on the assumption that all the semiconductor devices are identical with the same parasitics, and the transformer magnetizing current is negligible, but the DC-current in the transformer primary is considered. Each interval is modeled from the volt-second balance on the input and output inductors, as given in (1) to (8).

$$\phi_{2a} = \frac{(2nV_{in} - V_o)\phi_a}{V_o} \quad (1)$$

$$\phi_{2b} = \frac{(2nV_{in} - V_o)\phi_b}{V_o} \quad (2)$$

$$T_{i1} = \frac{\phi_a T_s}{2} \quad (3)$$

$$T_{i2} = \frac{(2nV_{in} - V_o)T_{i1}}{V_o} \quad (4)$$

$$T_{i3} = \frac{T_s}{2} - T_{i1} - T_{i2} \quad (5)$$

$$T_{i4} = \frac{\phi_b T_s}{2} \quad (6)$$

$$T_{i5} = \frac{(2nV_{in} - V_o)T_{i4}}{V_o} \quad (7)$$

$$T_{i6} = \frac{T_s}{2} - T_{i5} - T_{i4} \quad (8)$$

where V_{in} and V_o are the input and output voltages (V), n is the transformer turns ratio, T_s is the switching period (s), T_{i1} to T_{i6} are intervals of DCM operating modes 1 to 6 (s), ϕ_a is the phase-shift between PWM of devices S_1 and S_3 , and ϕ_b is the phase-shift between PWM of devices S_4 and S_2 .

Using the above equations, the steady-state DC voltage gain is modeled as

$$\frac{V_o}{V_{in}} = \frac{4n}{1 + \left[1 + \frac{16L_f}{R_o T_s \phi^2}\right]^{\frac{1}{2}}} \quad (9)$$

where L_f is the filter inductance (H), R_o is the load resistance (Ω), and $\phi = \frac{\phi_a + \phi_b}{2}$ is the average phase-shift between the two legs.

From (9), it can be inferred that when R_o is high, which is the case of light load condition, the DC voltage gain loses its linearity as the denominator becomes dominant. Therefore, the condition at which the converter operates in DCM is necessary to understand the behavior.

C. Condition for DCM operation

The load resistance R_o determines either CCM or DCM in the BBFB converter. $R_{o(bound)}$ defines the load resistance

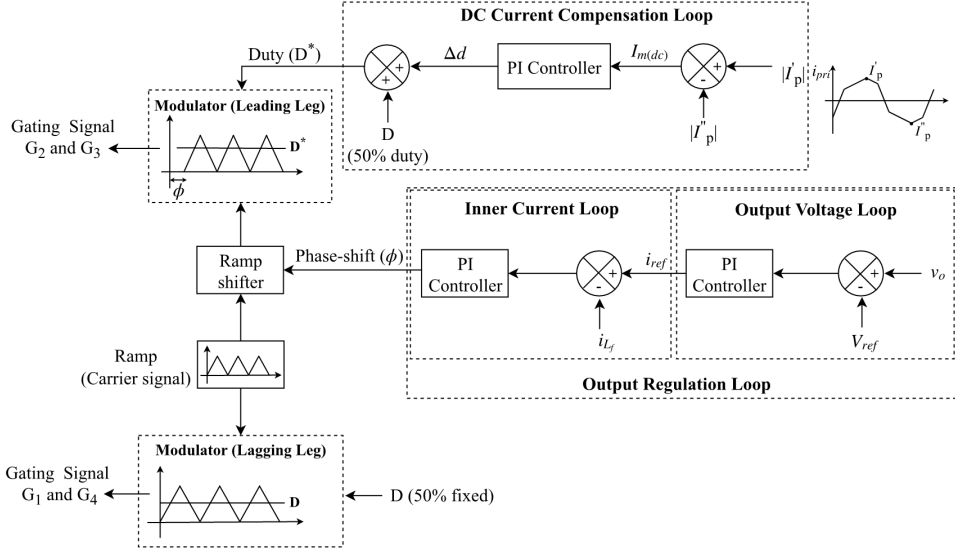


Fig. 2: HCS control block diagram

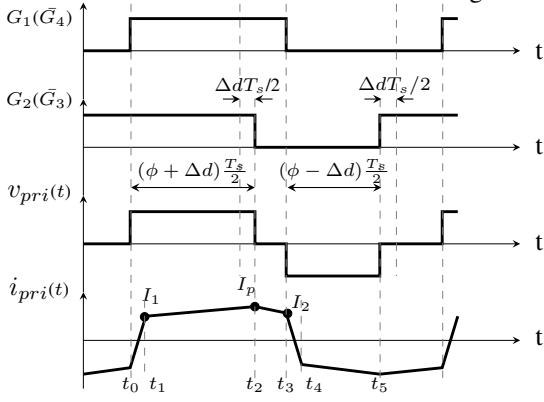


Fig. 3: Characteristic waveforms of BBFB with HCS

when BBFB operates at the boundary between CCM and DCM, which is given in (10). Therefore, when R_o is greater than $R_{o(bound)}$, BBFB operates in DCM and vice versa for CCM, as given in (11) to (13).

$$R_{o(bound)} = \frac{4L_f}{(1 - \phi_{eff})T_s} \quad (10)$$

$$R_o > R_{o(bound)} \quad DCM \quad (11)$$

$$R_o = R_{o(bound)} \quad \text{Boundary mode} \quad (12)$$

$$R_o < R_{o(bound)} \quad CCM \quad (13)$$

By knowing the boundary condition, the DC voltage gain of the converter for 0 to 100% load variations are plotted in Fig. 5, assuming $\phi=0.4$ and $n=12.6$ (as an example). Here, the gain in CCM is linear, while linearity is lost in DCM.

Due to non-linear behavior in DCM operation, it is preferred to operate BBFB in CCM for the complete load range, noting the derived boundary condition. Apart from the boundary condition, the BBFB converter design must also consider the ZVS range of the input devices to achieve higher efficiency

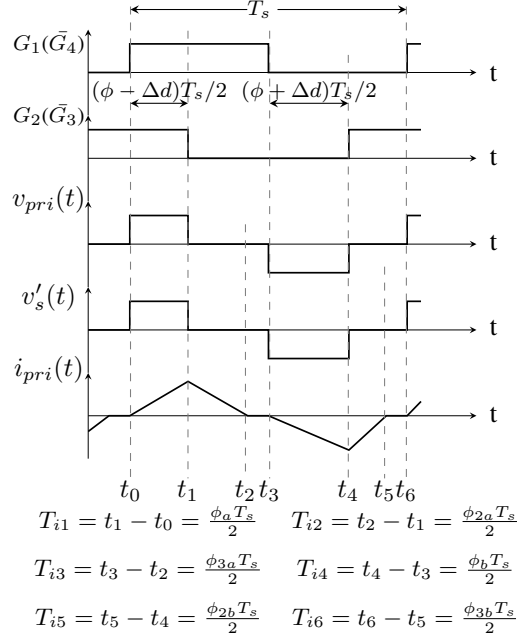


Fig. 4: Steady-state waveforms of BBFB in DCM

even at a light load condition.

D. ZVS range of MOSFETs S_1 to S_4

The ZVS switching of all the devices are advantages in various aspects such as, 1) reduced switching loss, 2) improved power density due to low loss, 3) better reliability of the converter, and 4) low EMI. The ZVS conditions for each device are different, however, which are derived in this section.

The ZVS condition for the leading leg MOSFETs S_2 and S_3 requires a non-zero transformer primary-side peak current during switching on condition, which is almost the case at all load conditions. Clearly, ZVS in the leading leg MOSFETs is

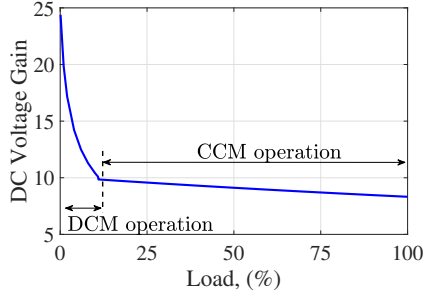


Fig. 5: DC voltage gain for the entire load range with constant $\phi = 0.4$ and $n = 12.6$

achieved under all load conditions. The ZVS conditions for the lagging leg MOSFETs S_1 and S_4 are different. The sum of input and transformer primary currents which flow through S_1 during turn on decides the ZVS operation. As a result, ZVS operation is possible even at a lighter load condition, as these currents are always positive and flow through the S_1 body diode, making the switch voltage to be zero.

For ZVS operation of S_4 , the current $I_{in} - i_{pri}(t_3)$ flowing through S_4 at turn-on instance (at the instant t_3 in Fig. 3) must be negative. Therefore, solving the ZVS requirement given in (14) results in a condition that the input voltage V_{in} must be larger than V_o/n , as given in (19). Interestingly, (19) indicates the ZVS operation of S_4 is V_{in} dependent, instead of load resistance.

$$I_{in} - i_{pri}(t_3) < 0 \quad (14)$$

$$I_{in} - I_2 < 0, \text{ as } i_{pri}(t_3) = I_2 \quad (15)$$

$$I_{in} < I_2 \quad (16)$$

$$2n\phi_{eff}I_o < nI_o \quad (17)$$

$$\phi_{eff} < 0.5 \quad (18)$$

$$\frac{V_o}{2nV_{in}} < 0.5, \text{ from voltage gain} \quad (19)$$

$$\text{where, } I_{in} = 2n\phi_{eff}I_o \\ I_2 = nI_o$$

where, $i_{pri}(t_3)$ is the transformer primary current at instance t_3 (A), I_{in} and I_o are the input and output currents, respectively (A).

The steady-state analysis presented in this section is validated in the next section. Additionally, the dynamic behavior of the HCS control is discussed with the results.

III. RESULTS AND DISCUSSIONS

This section presents the simulation and hardware experimental results to validate the BBFB converter's steady-state and dynamic models. The specification considered are 18-32 V input, 270 V output with 2 kW rated power. The BBFB converter is designed with the values $n=12.6$, $L_f=2$ mH, $\phi=0.29$, and $f_s=100$ kHz, following the guidelines given in [1]. Fig. 6 shows the BBFB converter experimental setup.

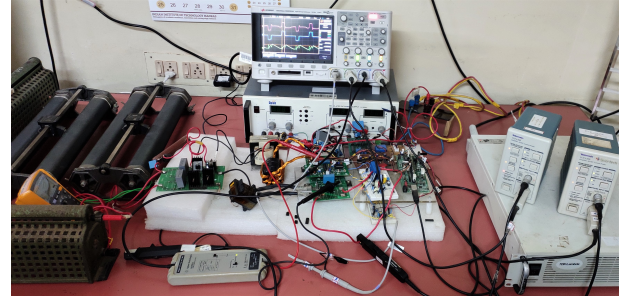
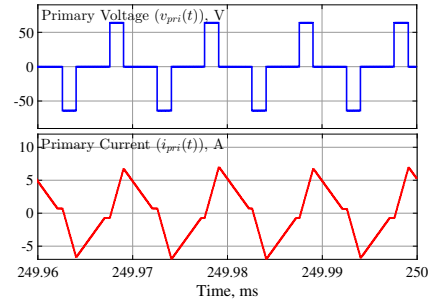


Fig. 6: BBFB converter experimental setup

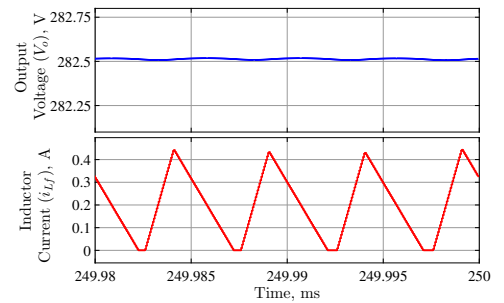
A. BBFB converter in DCM operation

For the designed values of L_f , ϕ , and T_s , the load resistance $R_{o(bound)}$ when the converter operates in boundary between CCM and DCM is evaluated to be 1129Ω , from (10).

To verify the conditions derived in (11) to (13), the BBFB converter is operated with a load resistance R_o of 1400Ω at 32 V input. Simulated transformer primary voltage and current waveforms are shown in Fig. 7(a), and output voltage and inductor current waveforms are shown in Fig. 7(b). From these results, the zero current period in the current waveforms indicates the DCM operation as $R_o > R_{o(bound)}$. Besides, the output voltage of 282.5 V at 29% phase-shift in Fig. 7(b) verifies the theoretically computed value of 284.06 V from the steady-state DCM voltage gain model derived in (9).



(a)



(b)

Fig. 7: Simulation results at 32 V input, 1400Ω load resistance with $\phi=0.29$ showing: (a) transformer primary voltage and current waveforms; (b) output voltage and inductor current waveforms

The DCM operation experimental results of the hardware

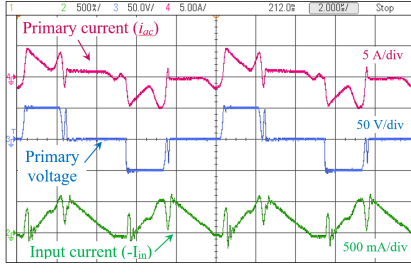
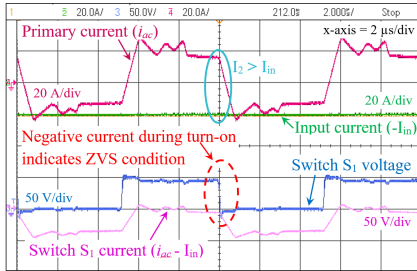


Fig. 8: Hardware experimental results: BFB characteristics waveforms at DCM

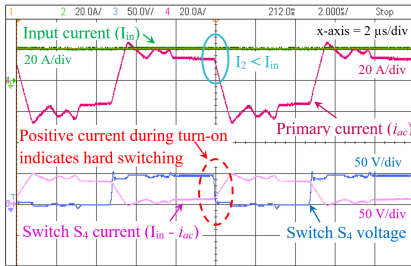
BFB converter from Fig. 6 is presented in Fig. 8. The results validate the DCM operation and characteristic waveforms discussed in the previous sections.

B. ZVS of semiconductor devices

As discussed earlier, the ZVS operation for switch S_4 depends on the effective phase-shift ϕ_{eff} , while for S_1 , ZVS is achieved at all the load conditions due to a negative current flow. To verify this, a switch's voltage and current as well as input and transformer primary currents at $\phi_{eff}=0.55$ are captured in the experiment as shown in Fig. 9(a) and Fig. 9(b), for S_1 and S_4 , respectively. As the ϕ_{eff} value violates the ZVS condition for S_4 , which must be < 0.5 as in (19), hard-switching occurs. To achieve ZVS in S_4 for the complete load range, the turns ratio n must be designed appropriately such that ϕ_{eff} is always less than 0.5.



(a) Switch S_1



(b) Switch S_4

Fig. 9: Experimental results: Switching transitions of the lagging leg switches S_1 and S_4 . Math channel (pink) indicates the respective switch currents

The oscillations seen in the transformer primary and switch currents are due to the parasitic capacitance effects, which is evaluated in the next subsection.

C. Parasitic effects in the current waveform

Oscillations in the transformer primary current during power transfer intervals, as seen in Fig. 9(a) and Fig. 9(b), occur due to the transformer leakage inductance L_{lk} , parasitic capacitances of the transformer C_{Tr} and output diodes C_{diode} . The oscillation frequency is derived as

$$f_{osci} = \frac{1}{2\pi [L_{lk}(C_{Tr} + 2C'_{diode})]^{1/2}} \quad (20)$$

where C'_{diode} is the reflected output diode capacitance on the primary side.

The oscillation frequency when $L_{lk}=0.4859 \mu\text{H}$, $C_{diode}=55 \text{ pF}$, and $C_{Tr}=15 \text{ nF}$ is theoretically computed as 1.86 MHz from (20). Simulation results in Fig. 10 meet the expectation showing a 1.92 MHz oscillation. On the other hand, the oscillations in the experimental results seen in Fig. 9(a) and Fig. 9(b) are about 1.3 MHz. The difference between the theoretical and experimental values is due to other unknown parasitic capacitances and inductance in the current path and PCB tracks.

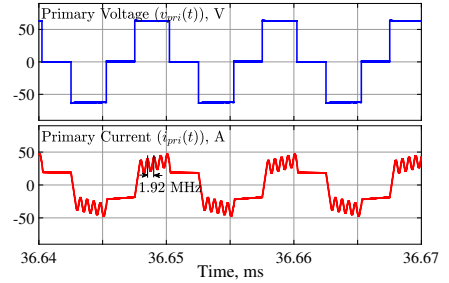


Fig. 10: Simulation: Transformer primary voltage and current waveforms showing the 1.92 MHz oscillation

D. Dynamic response of BFB with and without HCS control

The BFB converter uses the HCS control to mitigate the DC-current flowing through the transformer primary winding to avoid saturation. Ref [1] verifies that the HCS control does not interfere with the output voltage under a steady-state. However, as mentioned earlier, dynamic performance needs to be analyzed.

The small-signal transfer function of the transformer primary winding DC-current $\langle i_{DC} \rangle$ to the duty of the leading leg MOSFETs D^* is given as

$$\frac{\langle i_{DC} \rangle > T_s (s)}{D^*(s)} = \frac{2nVin}{sL_m + (R_{Tr} + 2R_{on})} \quad (21)$$

where L_m is the magnetizing inductance (H), R_{Tr} and R_{on} are the transformer winding and MOSFETs' on-state resistances (Ω), respectively.

As seen from (21), the small-signal model is a first-order transfer function, and hence a PI controller is sufficient to achieve the required dynamic performance.

To understand the HCS control's effects during dynamic conditions, the BFB converter is subjected to a step change

in load from 500 W to 2 kW with and without the HCS control scheme. The output voltage response in Fig. 11(a) verifies that the HCS control does not alter the dynamic response as both the curves coincide.

Fig. 11(b) shows the transformer DC-current step-response (same as the average transformer magnetizing current) with and without the HCS control. The result shows that the DC-current without HCS shifts to the new steady-state value of 42 A from 11 A as it is proportional to the input current. However, the DC-current with HCS remains zero in the new steady-state condition, though a peak of 2 A current is observed in the dynamic condition, which is negligible compared to the transformer primary RMS current. Therefore, these results verify that the HCS scheme does not affect the BBFB converter performance even during the dynamic conditions.

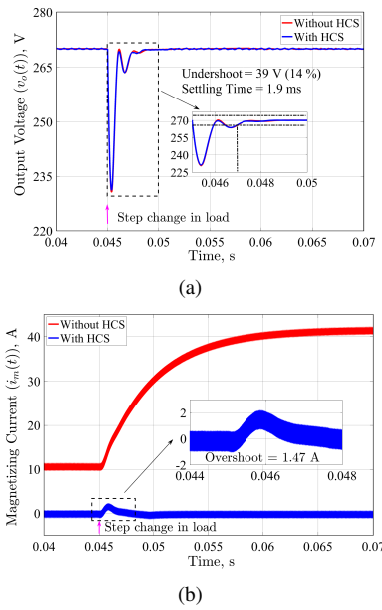


Fig. 11: Simulation results: Transient response of the BBFB converter with and without HCS control scheme for the load change from 500 W to 2 kW. (a) Output voltage response, (b) Magnetizing current response

IV. CONCLUSION

This paper presents a novel Buck-Boost full-bridge converter with the hybrid control scheme (HCS) and analyzes it extensively, including the CCM and DCM operations. The BBFB steady-state DC voltage gain model under DCM is derived. With the derived model, this work provides an insight for the DC voltage gain variations during CCM and DCM modes, which helps the designer choose the modes accordingly. The BBFB converter exhibits soft-switching during turn on, and the ZVS conditions are different from that of the conventional FB converters. Therefore, a model for the ZVS condition for all the four input switching devices is developed. Besides, this paper presents a model for the oscillation frequency seen in the practical transformer primary current due to the parasitics. Furthermore, the dynamic behavior of the HCS for the load step change is presented, which verifies that the HCS operation does not affect the output voltage, even under the dynamic

conditions. These derived models and analyses are verified in simulations and hardware experiments.

REFERENCES

- [1] N. Swaminathan and N. Lakshminarasamma, "Hybrid control scheme for mitigating the inherent DC-current in the transformer in buck-boost full-bridge converter for an all-electric motor drive system," *IET Power Electronics*, vol. 11, no. 8, pp. 1452–1462, 2018.
- [2] C. Li, Y. Zhang, Z. Cao, and D. XU, "Single-Phase Single-Stage Isolated ZCS Current-Fed Full-Bridge Converter for High-Power AC/DC Applications," *IEEE Transactions on Power Electronics*, vol. 32, no. 9, pp. 6800–6812, Sept 2017.
- [3] N. Swaminathan and Y. Cao, "An overview of high-conversion high-voltage dc-dc converters for electrified aviation power distribution system," *IEEE Transactions on Transportation Electrification*, vol. 6, no. 4, pp. 1740–1754, 2020.
- [4] J. A. Sabate, V. Vlatkovic, R. B. Ridley, F. C. Lee, and B. H. Cho, "Design considerations for high-voltage high-power full-bridge zero-voltage-switched PWM converter," in *Fifth Annual Proceedings on Applied Power Electronics Conference and Exposition*, March 1990, pp. 275–284.
- [5] A. Safaee, P. K. Jain, and A. Bakhshai, "An Adaptive ZVS Full-Bridge DC-DC Converter With Reduced Conduction Losses and Frequency Variation Range," *IEEE Transactions on Power Electronics*, vol. 30, no. 8, pp. 4107–4118, Aug 2015.
- [6] A. Mousavi, P. Das, and G. Moschopoulos, "A Comparative Study of a New ZCS DC-DC Full-Bridge Boost Converter With a ZVS Active-Clamp Converter," *IEEE Transactions on Power Electronics*, vol. 27, no. 3, pp. 1347–1358, March 2012.
- [7] W. J. Cha, J. M. Kwon, and B. H. Kwon, "Highly Efficient Asymmetrical PWM Full-Bridge Converter for Renewable Energy Sources," *IEEE Transactions on Industrial Electronics*, vol. 63, no. 5, pp. 2945–2953, May 2016.
- [8] M. C. Mira, Z. Zhang, A. Knott, and M. A. E. Andersen, "Analysis, Design, Modeling, and Control of an Interleaved-Boost Full-Bridge Three-Port Converter for Hybrid Renewable Energy Systems," *IEEE Transactions on Power Electronics*, vol. 32, no. 2, pp. 1138–1155, Feb 2017.
- [9] E. F. R. Romaneli and N. Barbi, "New isolated phase-shift controlled non-pulsating input and output converter," in *2001 IEEE 32nd Annual Power Electronics Specialists Conference*, vol. 1, 2001, pp. 237–242.
- [10] E. F. R. Romaneli and I. Barbi, "A new DC-DC converter with low current ripple characteristics," in *INTELEC. Twenty-Second International Telecommunications Energy Conference*, 2000, pp. 560–566.
- [11] E. F. R. Romaneli and I. Barbi, "An isolated ZVS-PWM active clamping nonpulsating input and output current DC-DC converter," in *2000 IEEE 31st Annual Power Electronics Specialists Conference. Conference Proceedings*, vol. 1, 2000, pp. 205–210.